HHS Public Access

Author manuscript

Hepatology. Author manuscript; available in PMC 2017 October 01.

Published in final edited form as:

Hepatology. 2016 October ; 64(4): 1317–1329. doi:10.1002/hep.28724.

Liver Kinase B1 regulates hepatocellular tight junction distribution and function *in vivo*

N Porat-Shliom[1,2,+], **AJ Tietgens**[3], **CM Van Itallie**[3], **L Vitale-Cross**[1], **M Jarnik**[4], **OJ Harding**[1], **JM Anderson**[3], **JS Gutkind**[1,5], **R Weigert**[1,2], and **IM Arias**[4]

[1]Oral and Pharyngeal Cancer Branch, National Institute of Dental and Craniofacial Research, National Institutes of Health, Bethesda, MD 20892

[2]Laboratory of Cellular and Molecular Biology, National Cancer Institute, National Institutes of Health, Bethesda, MD 20892

[3]Laboratory of Tight Junction Structure and Function, National Heart, Lung, and Blood Institute, Bethesda, MD 20892

[4]Cell Biology and Metabolism Program, Eunice Kennedy Shriver National Institute of Child Health and Human Development, National Institutes of Health, Bethesda, MD 20892

Abstract

Liver Kinase B1 (LKB1) and its downstream effector AMP-activated protein kinase (AMPK) play critical roles in polarity establishment by regulating membrane trafficking and energy metabolism. In collagen sandwich-cultured hepatocytes, loss of LKB1 or AMPK impaired apical ABCB11 (Bsep) trafficking, and bile canalicular formation. In the present study, we used liver-specific (Albumin-Cre) LKB1 knockout mice (LKB1−/−) to investigate the role of LKB1 in the maintenance of functional tight junction (TJ) *in vivo*. Transmission electron microscopy (TEM) revealed that hepatocyte apical membrane with microvilli substantially extended into the basolateral domain of LKB1 −/− livers. Immunofluorescence (IF) studies showed that loss of LKB1 leads to longer and wider canalicular structures correlating with mis-localization of the junctional protein, cingulin. To test junctional function, we used Intravital Microscopy (IVM) to quantify the transport kinetics of 6-carboxy-fluorescein diacetate (6-CFDA), which is processed in hepatocytes into its fluorescent derivative 6-carboxyfluorescein (6-CF) and secreted into the canaliculi. In LKB1 −/− mice, 6-CF largely remained in hepatocytes, canalicular secretion was greatly delayed and 6-CF appeared in the blood. To test whether 6-CF was transported through permeable TJ, we intravenously injected a low molecular weight (3kDa) dextran in combination with 6-CFDA. In wild type mice, 3kDa dextran remained in the vasculature whereas it rapidly appeared in the abnormal bile canaliculi in LKB1 −/− mice, confirming that junctional disruption resulted in paracellular exchange between the blood stream and the bile canaliculus.

[+]Correspondance: poratshliomn@mail.nih.gov, Natalie Porat-Shliom, PhD, Postdoctoral Research Fellow, Laboratory of Cellular and Molecular Biology, CCR - NCI, National Institutes of Health, Building 37, Room 2050B, Bethesda, MD 20892, Phone: 301 594 8545, Fax: 301 496 1966.

[5]Current Address, UC San Diego Moores Cancer Center, La Jolla, CA 92093

Conclusion—LKB1 plays a critical role in regulating maintenance of TJ and paracellular permeability, which may explain how various drugs, chemicals, and metabolic states that inhibit the LKB1/AMPK pathway, result in cholestasis.

Keywords

AMP-activated protein kinase (AMPK); Paracellular pathway; Tight junctions permeability; Intravital Microscopy (IVM)

Introduction

Hepatocytes have a unique polarized organization including up to three apical canalicular plasma membrane domains and a larger basolateral domain that faces the sinusoidal compartment of the hepatic vasculature. Segregation of these plasma membrane domains is achieved by formation of TJ between individual cells, which creates a paracellular diffusion barrier critical for proper organ function (1, 2). TJ are composed of transmembrane pore forming barrier proteins including claudins and occludin that are linked to peripheral scaffolding proteins, such as Zona Occludens-1 (ZO-1). In turn, scaffolding proteins bind to regulatory proteins, such as cingulin, and cytoskeletal proteins, including myosin, that connect the scaffold with microtubules and actin (2, 3) (scheme in Fig 3 A). TJ permeability is regulated under various physiological conditions (4). For example, vasopressin, epinephrine, and angiotensin increase TJ permeability in perfused rodent liver (5). A similar effect is observed in pancreas in response to cholinergic stimulation (6). Two general mechanisms for regulation of TJ permeability have been proposed. The first involves transcriptional regulation or post-translational modification of junctional proteins. The second involves changes in the actin cytoskeleton that modify intercellular junction contacts and permeability (4). While it is accepted that claudins determine the size, charge and conductance properties of the paracellular pathway (2) the mechanisms regulating flux in the intact liver and the signaling molecules involved are not known. *In vivo* hepatic permeability is inferred based on the differential secretion of fluid phase probes with differential size such as inulin and sucrose (7). However, direct visualization of paracellular transport in the intact liver has not been achieved.

The serine-threonine kinase and tumor suppressor LKB1 is a well-conserved key regulator of cell polarity, trafficking and metabolism (8–10). In an intestinal cell line, LKB1 induces polarity in the absence of cell-cell or cell-matrix cues (11), and is involved in establishment and maintenance of cell polarity in pancreas (12), neurons (13), bronchial epithelia (14) and cultured hepatocytes (15, 16). LKB1 activates a family of metabolic sensors called AMPK. In hepatocytes, activation of the LKB1-AMPK pathway enhanced bile canalicular formation, whereas inhibition resulted in loss of polarity and mis-localization of apical transporters such as Bsep (15–17). In MDCK cells and cultured hepatocytes, AMPK regulates TJ assembly and disassembly in response to calcium depletion (18, 19). LKB1-AMPK activation phosphorylates cingulin, a junctional component promoting interaction with microtubules (20). However, whether and how the LKB1-AMPK pathway functions in the maintenance of established hepatocyte TJs in intact animals are not known.

Due to the importance of TJ in cell polarity and the involvement of LKB1 in hepatocyte polarization, we investigated the role of LKB1 in TJ regulation and function in the intact liver. Using a combination of TEM, IF and IVM to directly visualize biliary and paracellular transport, we demonstrate that LKB1 is central for the regulation and maintenance of TJ structure and function in the intact liver.

Material and Methods

Reagents and Antibodies

Catalogue numbers for commercially available antibodies are indicated in parentheses. The rat monoclonal antibody against ZO-1 clone R40.76 was used (21). Antibodies against Claudin-1 (71–7800), Claudin-3 (34–1700), Rab11a (71–5300) and Rhodamine phalloidin were from Thermo Fisher Scientific (Waltham, MA). The rabbit polyclonal antibody against Par-3 was from Milipore (07–330; Billerica, MA). The rabbit polyclonal antibody against Bsep was from Kamiya Biomedical Company (MC-333; Tukwila, WA). The rabbit antibody against cingulin was a gift from Dr. Sandra Citi (University of Geneva) (22) and the Myosin Vb was from Dr. John Hammer (NHLBI, NIH) (23). Rabbit anti-LKB1 (CST3047), anti-AMPK (CST2532), anti-phospho-Thr172 AMPK (pAMPK; CST2535) antibodies were purchased from Cell Signaling Technology (Danvers, MA). Mouse anti-alpha-tubulin (T6199) was from Sigma-Aldrich.

Liver-specific LKB1 −/− mice

The generation and maintenance of liver-specific LKB1 −/− mice (NCI mouse repository; MGI: 2387402) have been described before (17, 24). Briefly, Liver-specific LKB1 knockouts were obtained by crossing mice containing floxed LKB1 alleles with mice expressing the Cre recombinase under the control of Albumin promoter, Alb-Cre (The Jackson Laboratory; MGI: 2176228). Homozygous LKB1 knockouts (LKB1 −/−) and their wild type littermates (Control) were used in all experiments. Alb-Cre LKB1 −/− mice appear smaller in size than normal and as early as 10 days post birth display jaundice of the paws and snout. The animals were closely monitored. Animals displaying signs indicative of distress were euthanized. The study was approved and conducted according to the animal protocols approved by the Animal Care and Use Committee (ACUC), protocol 14–738 and 15–779, National Institute of Dental and Craniofacial research (NIDCR), in compliance with the “Guide for the Care and Use of Laboratory Animals” (NIH publication 86–23 revised 1985). Male and female mice, 7 or 21–23 days old, were used in experiments.

Tissue sections and Immunofluorescence

Livers were excised and snap frozen in liquid nitrogen. Frozen sections were prepared by the National Heart, Lung, and Blood Institute Pathology Core. Tissue sections were fixed in 100% methanol for 20 min at −20°C and then rehydrated in phosphate-buffered saline (PBS) for 30 min at 4°C. Sections were blocked in PBS containing 1% bovine serum albumin (BSA) and 5% normal goat serum (NGS) for 20 min at room temperature, followed by incubation with primary antibodies for 60 min at room temperature. Sections were washed three times for 10 minutes with the blocking solution, followed by incubation with fluorescent-labeled secondary antibodies (Cy2, Cy3 or Cy5-labeled, Jackson

Immunoresearch) for 60 min at room temperature. Sections were washed and mounted with Mowiol 4–88 (Sigma Aldrich; 81381) containing 1% n-propyl gallate. For Rab11a and phalloidin labeling with ZO-1, tissue sections were fixed in 1% paraformaldehyde in CSK buffer (10 mM 1,4-piperazinediethanesulfonic acid, pH 6.8, 100 mM KCl, 300 mM sucrose, 2 mM MgCl2, and 2 mM ethylene glycol tetraacetic acid) for 20 min at 4°C, permeabilized with 0.2% Triton X-100 (10 min), quenched with 50 mM NH4Cl (10 min) and blocked in 2% NGS in PBS for 60 min. Primary and secondary antibody incubations were performed as above.

Western Blot Analysis

Frozen liver tissue was lysed in RIPA buffer (150 mM NaCl, 0.1% Triton X-100, 0.5% sodium deoxycholate, 0.1% SDS, and 50 mM Tris-HCl pH 8.0) containing protease inhibitor cocktail, and homogenized using ceramic beads with electric tissue homogenizer (Bertin Technologies) at 5000 rpm for 20 seconds, followed by centrifugation at 13,000 rpm at 4° for 20 minutes. 20 μg of protein were separated on 4–20% gel (BIO-RAD) SDS-PAGE at 100V for 90 minutes. Proteins were transferred on ice for 1 hour at 100V to nitrocellulose membrane, which was subsequently blocked in 5% milk-TBS for 1 hour. Membranes were incubated with primary antibodies overnight at 4°, followed by washing in TBST, and incubation with secondary HRP-conjugated antibodies for 1 hour at room temperature. Membranes were washed again with TBST before protein was detected with SuperSignal West Femto Maximum Sensitivity Substrate (Thermo Scientific, Waltham, MA). Films were scanned using EPSON Perfection V700 scanner and quantification of band densitometry was measured with ImageJ standard gel analysis. Mean ± SD was calculated from three individual experiments and Student's t-test was used for calculation of the p-value.

Transmission Electron Microscopy

Small liver samples (1 mm^3 max) were fixed for 1.5 h in 2% (wt/vol) formaldehyde and 2% (wt/vol) glutaraldehyde in 0.1 M sodium cacodylate (pH 7.2), postfixed in 1% aqueous OsO4, and stained en bloc with 2% (wt/vol) uranyl acetate. Samples were further dehydrated with series of ethanol concentrations, penetrated with EMbed 812 (Electron Microscopy Sciences) and placed in flat molds. The resin was subsequently polymerized at 65 °C for 60 h. Thin (70-nm) sections were cut using a Leica EM UC7 microtome and subsequently were stained with uranyl acetate and lead citrate. The samples were examined on an FEI Tecnai 20 TEM operated at 120 kV, and images were recorded on an AMT CCD camera.

Intravital Microscopy of the Liver

Mice at 21–23 days after birth were anesthetized by an intraperitoneal (IP) injection of 100 mg/Kg ketamine (Fort Dodge Animal Health, Fort Dodge, IA) and 20 mg/Kg xylazine (Akorn Inc., Decatur, IL) for control (approximately 8 gr) and 25mg/Kg ketamine and 5mg/Kg xylazine for LKB1 −/− (approximately 4 gr). Body temperature was monitored using a rectal probe. 20U of heparin were injected IP to avoid ischemia. The tip of the left lateral lobe of the liver was exposed by 2–3 cm incision made along the ribcage. Following cutting of the skin, the muscle was cut using a cauterizer to avoid bleeding. Incision was cooled with wet gauze. Qtracker 655 Vascular Label (ThermoFischer Scientific, Waltham, MA) was injected retro-orbital, 20μl per mouse, to visualize sinusoids and blood flow. For

positioning of the mouse on the microscope stage, a cardboard with a rectangle window large enough to surround the exposed lobe was taped to the microscope stage, which reduced motion artifacts due to heartbeat and respiration. The liver lobe was separated with a narrow gauze strip followed by application of water based 0.3% carbomer 940 gel (Snowdrift farm, Tucson, AZ also available from Lubrizon Wickliffe, Ohio) to prevent tissue dehydration during imaging. Additional fluorescent probes were administered through retro-orbital injection including 0.2μg/gr 6-Carboxyfluorescein diacetate (Sigma-Aldrich) or 3kDa Texas Red dextran (ThermoFischer Scientific, Waltham, MA), 30ul in control and 20ul in LKB1 −/−, as noted. Imaging was done as described before using IX81 inverted confocal microscope equipped with a Fluoview 1000 scanning head (OlympusAmerica) (25). 6-CF and Alexa 488 were excited with a 488-nm laser, Texas Red–dextran and Alexa 594 were excited with a 561-nm laser, and Qtracker 655 was excited with a 633-nm laser. For the time-lapse imaging, 20μm stacks with 1μm step size were acquired every 2 minutes over the course of up to an hour. Time-lapse series were acquired using a UPLSAPO 40XS, 40X N.A. 1.25 silicon oil objective (Olympus America).

Image Analysis and Quantification

Original OIF files were opened in ImageJ and corrected for 3D drift as necessary. Quantification of canaliculi width and length was performed on maximal projections of 5μm z-stacks using ImageJ. At least three stacks from two independent control or LKB1 −/− were used and 30–45 cells analyzed. The shortest distance between two opposite ZO-1 positive junctions (for canalicular width) or the maximal continuous ZO-1 labeling (for canalicular length) were measured. For canalicular width/length per cell, values obtained were summed and divided by the number of cells.

To measure 6-CF transport, sum-projections were generated using ImageJ, background was subtracted and 6-CF mean fluorescence was measured. Fluorescence over time was plotted as Mean ± SEM (control n=4; LKB1−/− n=3; Fig 3 B). To address the relationship between 6-CF and Qtracker 655 vascular label, stacks of images collected over time were analyzed in 4D with Imaris software v7.6.3 (Bitplane, Belfast, UK). Quantification of co-localization was assessed in 3D, and pixel co-distribution was calculated for green and red fluorescent patterns. The degree of co-localization of 6-CF (green) and Qtracker (red) was quantified and expressed as Pearson co-localization coefficient (1, perfect correlation or perfect co-localization; 0, no correlation; −1, perfect inverse correlation). For measurements of paracellular transport, twenty 10×10μm squares were drawn, using ImageJ, in canalicular area based on 6-CF fluorescence. The regions were transferred to the 3kDa dextran channel and mean intensity was measured. Mean and standard deviation over time of normalized mean fluorescence were calculated and presented in the graph. Similar results were obtained from three independent experiments and a representative graph is presented.

Results

Loss of LKB1 leads to abnormal bile canalicular morphology

Liver specific LKB1 knock out mice (LKB1 −/−) exhibit a severe phenotype including weight loss, dehydration and jaundice, and die approximately 28 days after birth (17, 24).

Therefore, mice at 21–23 days after birth were used in this study. Despite their clinical condition, Haematoxylin and Eosin staining (H&E) of LKB1 −/− liver sections showed no sign of inflammation or necrosis compared with controls (24) (and Fig 1 A) thus suggesting that the severe phenotype results from depletion of LKB1 in hepatocytes and is not secondary to hepatocellular necrosis or inflammation.

TEM studies were performed for qualitative evaluation of canalicular morphology. In 1-week old control and LKB1 −/− mice canalicular channels, well-defined canaliculi, microvilli, and TJs were observed (Fig 1 B) consistent with the fact that LKB1 protein depletion is initially detected 10–14 days after birth (17, 24). Similarly, liver sections from 3-week-old control mice displayed normal morphology including clearly identified TJs (Fig 1 C upper panel). However, in LKB1 −/− liver sections, TJs were reduced in number and difficult to recognize (Fig 1 C lower panel). The canalicular spaces substantially extended into the lateral membrane domain of the hepatocytes (Fig 1 D). Bile canaliculi with normal appearance were occasionally observed in LKB1 −/− mice due to regional heterogeneity.

LKB1 depletion results in disrupted TJ structure and mis-localization of cingulin

To investigate the role of LKB1 in TJ maintenance in hepatocytes, we initially evaluated the distribution of ZO-1, which links junctional barrier proteins, such as claudins, to the actin cytoskeleton (2) (Fig 2). Liver tissue sections from control and LKB1 deficient mice were processed for IF as described in Material and Methods. ZO-1 staining labeled the borders of the canaliculi in control mice with the typical linear morphology. However, in LKB1 −/− mice, ZO-1 staining was tortuous and disorganized. Quantification of canalicular morphology based on ZO-1 labeling revealed that LKB1 −/− mice have significantly longer and wider canaliculi when compared with control (Fig 2).

To evaluate further TJ structure, we examined the distribution of filamentous actin using phalloidin labeling. As expected, the actin cytoskeleton was primarily associated with TJ in control liver sections and co-localized with ZO-1 staining (Fig 3 A and B). In the absence of LKB1, actin co-localization with ZO-1 was unchanged although, similar to ZO-1 staining, it revealed the disrupted morphology and distribution of the junctions (Fig 3 B). Next we labeled the transmembrane TJ protein, Claudin-1. In control sections, Claudin-1 had a linear pattern similar, but not overlapping, with ZO-1 consistent with the fact that the former is a transmembrane apical protein and the latter is cytosolic. In LKB1 −/− Claudin-1 showed disorganized distribution highlighting the significantly wider canaliculi and was also observed in internal compartments (Fig 3 C). Similar distribution was observed for Claudin-3 (Sup Fig 1 A). The regulatory protein cingulin links TJ with the cytoskeleton, regulates signal transduction (26) and has been identified as an AMPK effector (20, 27). In control liver sections, cingulin localized in close proximity with ZO-1 at TJ. However, in LKB1 −/− sections, cingulin was infrequently associated with TJ and was predominantly cytosolic (Fig 3 D). Western blot analysis of phosphorylated AMPK levels revealed a significant reduction in phosphorylated AMPK levels in the absence of LKB1, which may explain the altered distribution of cingulin (Fig 3 E).

Previous reports noted the delayed trafficking of the apical transporter Bsep in the absence of LKB1 (17, 24). In control liver sections, Bsep localized to apical membranes whereas

ZO-1 highlighted the adjacent TJ (Sup Fig 1 B). In the absence of LKB1, Bsep was observed in internal compartments and only partially localized to apical membranes (Sup Fig 1 B). Additionally, residual Bsep that was properly transported to the apical membrane highlighted the much-widened apical domain (Sup Fig 1 B). β-catenin, a major component of adherens junctions, had comparable distribution in control and LKB1 −/− mice (Sup Fig 1 C).

LKB1 regulates polarity in part through the regulation of membrane trafficking (17, 28). Therefore we determined the distribution of Rab11a and Myosin Vb (recycling endosomes) and Par-3 (polarity regulating protein). Under control conditions, Rab11a and Myosin Vb are localized in apical recycling endosomes adjacent to apical membranes whereas Par3 localized to TJ with ZO-1. Loss of LKB1 revealed only minor changes in their distribution (Sup Fig 1 D–F).

Our findings show that the TJ proteins Claudin-1, Claudin-3 and actin remained associated with the abnormal junctions in the absence of LKB1, whereas cingulin lost association with TJ and became mostly cytosolic.

Delayed canalicular secretion in LKB1 deficient mice

To test junctional barrier function, we adopted a previously described method to evaluate efflux transporter activity using 6-carboxyfluorescein diacetate (6-CFDA) and IVM (29, 30). 6-CFDA is a non-fluorescent, membrane permeant probe. Deacetylation of 6-CFDA in the cytosol of hepatocytes yields a fluorescent, charged molecule, 6-carboxyfluorescein (6-CF) that is visible and membrane impermeant. Consequently, 6-CF is secreted into the bile canaliculi by ABCC2 and fluorescence can be used to quantitatively measure transporter activity.

For IVM, control and LKB1 −/− mice were anesthetized and the left lobe of the liver was exposed as described in Materials and Methods. Prior to imaging, the vascular label Qtracker 655 was injected retro-orbitally to evaluate blood flow and identify regions for imaging. For time-lapse imaging, 20μm stacks were acquired every 2 minutes for up to an hour. 0.2 mg/kg 6-CFDA was retro-orbitally injected following the acquisition of the first stack. Fig 4 A shows single frames from control or LKB1 −/− representative time lapses. For quantification of 6-CF fluorescence over time, sum-projections were generated using ImageJ, as described in Material and Methods. Mean fluorescence of 6-CF from entire frames over time, was plotted as Mean ± SEM (control n=4; LKB1−/− n=3; Fig 3 B). In control mice, 6-CF fluorescence increased sharply in the first 2 minutes and peaked at 4–6 minutes (Fig 4 B). Fluorescence originated from both hepatocytes cytosol and bile canaliculi (Fig 4 A). Subsequently, a gradual decrease in fluorescence was observed representing transport of 6-CF from the cytosol into the canaliculus followed by excretion and loss of 6-CF signal by 50 minutes after injection (not shown). In LKB1 −/− mice, 6-CF largely remained in hepatocytes (compare 6-CF fluorescence at 34 minutes after injection in control and LKB1 −/−); its secretion was greatly delayed likely due to mis-localization of the transporter. The lower fluorescence intensity observed in LKB1 −/− mice could be due to changes in pH. Surprisingly, although 6-CF excretion was delayed, green fluorescence appeared in the

blood and accumulated over time (Fig 4 A inset). This was confirmed in co-localization analysis of 6-CF with respect to the vasculature marker (Qtracker 655). Following the analysis, Pearson's coefficient was calculated (1, perfect correlation or perfect co-localization; 0, no correlation; −1, perfect inverse correlation). Figure 4 C presents the Pearson's coefficient values from one control mouse and one LKB1 −/− mouse, over the course of the respective experiments. In the control, Pearson's coefficient values ranged from −0.0858 to −0.0039 indicating no correlation between the two channels. In the LKB1 −/− mouse, the range was 0.2243 to 0.4097. Notably, LKB1 −/− mice had relatively high basal Pearson's coefficient values due to elevated serum bilirubin levels resulting in background fluorescence (17, 24). However, Pearson's coefficient increased over time demonstrating increased co-localization of 6-CF labeling with Qtracker. This overall trend was observed in four control and three LKB1 −/− mice as shown in Figure 4 D.

Theoretically, 6-CF may be transported from hepatocytes directly back to the blood or diffuse from the canalicular space through permeable TJ. We previously showed that expression of the basolateral ABCC3 and ABCC4, which can transport organic anions from liver into the circulation, was not induced (17). Therefore, we postulated that 6-CF might be returned to the circulation through permeable TJs via the paracellular pathway.

LKB1 regulates paracellular permeability in the liver

To test the possibility that permeability of TJs increase in the absence of LKB1, we modified the previously described IVM approach by adding a low molecular weight Texas red-dextran (3kDa; Stokes radius 2.6 nm (31)). If TJs are permeable and solutes can diffuse from the bile canaliculi into the blood, then the 3kDa dextran injected systemically would have access into the canalicular space.

To explore this possibility, control and LKB1−/− mice livers were imaged *in vivo*. Blood flow was visualized using Qtracker 655 followed by injection of 6-CFDA to identify canaliculi, and 3kDa dextran to evaluate TJ permeability (32). In control mice, 3kDa dextran remained in the vasculature throughout the experiment and was never observed to coincide with 6-CF in the canalicular space (Fig 5 and Movie S3). However, in LKB1 −/− liver, 3kDa dextran rapidly (2 minutes after injection) appeared in the canalicular space and accumulated over time (Fig 5 and Movie S4). Quantification of 3kDa dextran fluorescence in the canalicuar area was measured based on 6-CF accumulation and intensity over time shows that while 3kDa dextran does not accumulate in the canalicular space in control mice, it rapidly increases in LKB1 −/−. These results indicate that LKB1 may be involved in the regulation of paracellular permeability.

Discussion

AMPK is a key substrate of LKB1. Following phosphorylation of threonine 172, active AMPK regulates multiple metabolic effects including polarity and mitochondrial dynamics (33). AMPK activates a large number of downstream targets including cingulin (20, 27) Par-1 (34) and CLIP170, a plus end microtubular protein (35). In addition, AMPK indirectly regulates ATP synthesis by mitochondria by increasing cellular glucose uptake and

glycolysis (10), and up regulating mitochondrial biogenesis (36), and directly by regulating mitochondrial fusion to enhance ATP synthesis by oxidative phosphorylation (37–39). Notably, AMPK phosphorylation was significantly reduced in LKB1 −/− mouse liver (Fig 3 E). Therefore, although several mechanisms may be responsible for the multiple cellular effects observed after LKB1 depletion, it is likely that AMPK is responsible for the observed effects on TJ structure and function.

TJ structure and regulation are complex, reviewed elsewhere (2) and schematized in Figure 3 A. Notably, TJ create the functional barrier, which restricts paracellular movement of water and solutes between blood and bile (2, 4, 40). Transmembrane proteins seal TJ by interacting with partners on adjacent cells and also bind directly to the scaffolding protein ZO-1 at the TJ. In turn, ZO-1 directly binds to peri-junctional F-actin and other components of the cytoskeleton and is proposed to coordinate barrier function with cytoskeletal changes (41). Dynamic coupling between the barrier and the cytoskeleton is presumably required since the TJ must maintain an Ångström-level paracellular seal in the face of continuous intercellular movements, apoptosis, and epithelial restitution (42). Although the physiological cues that lead to LKB1 activation are not known, it is possible that signaling pathways downstream of LKB1 regulate paracellular flux via changes in actin organization, actomyosin contractility, or occludin (43, 44).

Extensive TEM study of liver specimens revealed substantial paucity of bile canaliculi and TJ in LKB1 deficient mice. Remarkably, this was associated with extension of bile canaliculi with abundant microvilli into the normal lateral plasma membrane domain at one or both borders of the canalicular membrane. While major disruptions in canalicular morphology were observed, the TJ components investigated show only modestly diminished fidelity in their subcellular localization with the exception of cingulin. Cingulin, which is an AMPK target (27), and associates with microtubules in response to AMPK phosphorylation (20), loses TJ localization and is widely distributed throughout the cytoplasm (Fig 3 D). In contrast, ZO-1, Claudin-1, Claudin-3 and actin remain mostly associated with the residual canalicular structures and show only minor redistribution to other areas of the cell (Fig 2, Fig 3 B–C and Sup Fig 1 A). Detailed mechanistic study of the role of LKB1 in TJ function will require substantial studies beyond the scope of the present report.

The phenotype observed in LKB1 −/− mice is primarily functional and not associated with hepatocellular necrosis or inflammation (24) and Fig 1 A. The major effects are metabolic probably involving the multiple roles of AMPK (36) and are manifested by weight loss and death. Jaundice also largely results from canalicular and junctional defects (45). Various experimental and clinical cholestatic disorders are associated with increased expression of ABCC3 and C4, which localize to the sinusoidal plasma membrane domain of hepatocytes and facilitate transport of retained conjugated bilirubin from liver back into the circulation. In LKB1 −/− mouse liver, expression of these normally quiescent transporters was not increased (17). An alternative or additional mechanism by which conjugated bilirubin can be transferred from bile into the circulation is through permeable TJs via the paracellular pathway. Interestingly, Petzelbauer and colleagues recently demonstrated that cingulin regulates endothelial barrier function and that loss of cingulin from TJ results in increased junctional permeability (46).

Demonstration and quantification of the paracellular pathway in liver is rendered difficult due to instability of hepatocyte cultures. In perfused liver, the paracellular pathway is examined by calculating plasma to bile ratio of fluid phase probes varying in size (7). To date, no direct visualization and measurement of hepatic TJ permeability have been demonstrated *in vivo*. The present study demonstrates direct dynamic transfer of 3kDa dextran from the blood to the canalicular space in LKB1 −/− liver but not in control mouse liver (Fig 5). These observations reveal paracellular permeability and are consistent with appearance of 6-CF in sinusoidal blood following its uptake and secretion by hepatocytes in LKB1 −/− mouse liver (Fig 4 A inset and C). The Stokes radius of 3kDa dextran is 2.6 nm (31), indicating that the TJ opening in LKB1 −/− mouse liver exceeds this dimension. It may be possible to quantify TJ permeability change using dextrans of different sizes.

IVM of liver was initially described in the early 1950s by Hanzon (47), but was subsequently neglected. Technical advances in microscopy, deep tissue imaging, fluorescent probes, transgenic animal models and image analysis have made possible in situ studies of subcellular, cellular and tissue processes within a living organism (30, 48). Importantly, concepts derived from cell cultures and other species can be evaluated at the organ level under varied developmental, experimental and genetic conditions. In the present study, we used transgenic LKB1 −/− mice; however, virtually any transgenic mouse can be similarly studied under varied experimental conditions. Finally, IVM offers an opportunity to bridge the knowledge gap between the cell, organ and organism to better understand physiological and pathological processes.

The present study reveals that LKB1 is essential for regulating TJ and paracellular permeability. These findings are relevant to the pathogenesis of cholestasis induced by drugs, chemicals, viruses and metabolic states, which inhibit the LKB1 pathway.

Supplementary Material

Refer to Web version on PubMed Central for supplementary material.

Acknowledgments

Financial Support: This research was supported by the Intramural Research Program of the NIH, National Institute of Dental and Craniofacial Research.

This research was supported by the Intramural Research Program of the NIH, National Institute of Dental and Craniofacial Research. We thank Dr. Julie Donaldson, NHLBI for critical reading the manuscript and Daniela Malide, NHLBI light microscopy core for helping with co-localization analysis. Liver IVM protocol was developed and optimized with Kirstin Meyer form the Max Planck Institute, Dresden.

List of abbreviations

AMPK	AMP-activated protein kinase
LKB1	Liver Kinase B1
TJ	Tight Junction
TEM	Transmission electron microscopy

Bsep	Bile Salt Export Pump
ABCB11	ATP Binding Cassette protein B11
Alb-Cre	Albumin-Cre
6-CFDA	6-carboxy-fluorescein diacetate
6-CF	6-carboxyfluorescein
3kDa	three kilo Dalton
ZO-1	Zona Occludens-1
TER	transepithelial electrical resistance
IVM	Intravital Microscopy
IF	Immunofluorescence
H&E	Haematoxylin and Eosin

References

1. Treyer A, Musch A. Hepatocyte Polarity. Comprehensive Physiology. 2013; 3:243–287. [PubMed: 23720287]
2. Van Itallie CM, Anderson JM. Architecture of tight junctions and principles of molecular composition. Semin Cell Dev Biol. 2014; 36:157–165. [PubMed: 25171873]
3. Furuse M. Molecular basis of the core structure of tight junctions. Cold Spring Harb Perspect Biol. 2010; 2:a002907. [PubMed: 20182608]
4. Turner JR, Buschmann MM, Romero-Calvo I, Sailer A, Shen L. The role of molecular remodeling in differential regulation of tight junction permeability. Semin Cell Dev Biol. 2014; 36:204–212. [PubMed: 25263012]
5. Lowe PJ, Miyai K, Steinbach JH, Hardison WG. Hormonal regulation of hepatocyte tight junctional permeability. Am J Physiol. 1988; 255:G454–461. [PubMed: 2845804]
6. Kuijpers GA, Van Nooy IG, Vossen ME, Stadhouders AM, Van Uyen A, De Pont JJ, Bonting SL. Tight junctional permeability of the resting and carbachol stimulated exocrine rabbit pancreas. Histochemistry. 1985; 83:257–264. [PubMed: 4044311]
7. Lake JR, Licko V, Van Dyke RW, Scharschmidt BF. Biliary secretion of fluid-phase markers by the isolated perfused rat liver. Role of transcellular vesicular transport. J Clin Invest. 1985; 76:676–684. [PubMed: 2411761]
8. Jansen M, ten Klooster JP, Offerhaus GJ, Clevers H. LKB1 and AMPK Family Signaling: The Intimate Link Between Cell Polarity and Energy Metabolism. Physiological Reviews. 2009; 89:777–798. [PubMed: 19584313]
9. Baas AF, Smit L, Clevers H. LKB1 tumor suppressor protein: PARtaker in cell polarity. Trends in Cell Biology. 2004; 14:312–319. [PubMed: 15183188]
10. Shaw RJ, Lamia KA, Vasquez D, Koo SH, Bardeesy N, Depinho RA, Montminy M, et al. The kinase LKB1 mediates glucose homeostasis in liver and therapeutic effects of metformin. Science. 2005; 310:1642–1646. [PubMed: 16308421]
11. Baas AF, Kuipers J, van der Wel NN, Batlle E, Koerten HK, Peters PJ, Clevers HC. Complete polarization of single intestinal epithelial cells upon activation of LKB1 by STRAD. Cell. 2004; 116:457–466. [PubMed: 15016379]
12. Hezel AF, Gurumurthy S, Granot Z, Swisa A, Chu GC, Bailey G, Dor Y, et al. Pancreatic LKB1 deletion leads to acinar polarity defects and cystic neoplasms. Molecular and Cellular Biology. 2008; 28:2414–2425. [PubMed: 18227155]

13. Shelly M, Cancedda L, Heilshorn S, Sumbre G, Poo MM. LKB1/STRAD promotes axon initiation during neuronal polarization. Cell. 2007; 129:565–577. [PubMed: 17482549]
14. Xu X, Jin D, Durgan J, Hall A. LKB1 controls human bronchial epithelial morphogenesis through p114RhoGEF-dependent RhoA activation. Molecular and Cellular Biology. 2013; 33:2671–2682. [PubMed: 23648482]
15. Fu D, Wakabayashi Y, Ido Y, Lippincott-Schwartz J, Arias IM. Regulation of bile canalicular network formation and maintenance by AMP-activated protein kinase and LKB1. J Cell Sci. 2010; 123:3294–3302. [PubMed: 20826460]
16. Fu D, Wakabayashi Y, Lippincott-Schwartz J, Arias IM. Bile acid stimulates hepatocyte polarization through a cAMP-Epac-MEK-LKB1-AMPK pathway. Proceedings of the National Academy of Sciences of the United States of America. 2011; 108:1403–1408. [PubMed: 21220320]
17. Homolya L, Fu D, Sengupta P, Jarnik M, Gillet JP, Vitale-Cross L, Gutkind JS, et al. LKB1/AMPK and PKA Control ABCB11 Trafficking and Polarization in Hepatocytes. Plos One. 2014:9.
18. Zheng B, Cantley LC. Regulation of epithelial tight junction assembly and disassembly by AMP-activated protein kinase. Proceedings of the National Academy of Sciences of the United States of America. 2007; 104:819–822. [PubMed: 17204563]
19. Zhang L, Li J, Young LH, Caplan MJ. AMP-activated protein kinase regulates the assembly of epithelial tight junctions. Proc Natl Acad Sci U S A. 2006; 103:17272–17277. [PubMed: 17088526]
20. Yano T, Matsui T, Tamura A, Uji M, Tsukita S. The association of microtubules with tight junctions is promoted by cingulin phosphorylation by AMPK. J Cell Biol. 2013; 203:605–614. [PubMed: 24385485]
21. Anderson JM, Stevenson BR, Jesaitis LA, Goodenough DA, Mooseker MS. Characterization of ZO-1, a protein component of the tight junction from mouse liver and Madin-Darby canine kidney cells. J Cell Biol. 1988; 106:1141–1149. [PubMed: 2452168]
22. Citi S, Sabanay H, Jakes R, Geiger B, Kendrick-Jones J. Cingulin, a new peripheral component of tight junctions. Nature. 1988; 333:272–276. [PubMed: 3285223]
23. Nedvetsky PI, Stefan E, Frische S, Santamaria K, Wiesner B, Valenti G, Hammer JA, et al. A role of myosin Vb and Rab11-FIP2 in the aquaporin-2 shuttle. Traffic. 2007; 8:110–123. [PubMed: 17156409]
24. Woods A, Heslegrave AJ, Muckett PJ, Levene AP, Clements M, Mobberley M, Ryder TA, et al. LKB1 is required for hepatic bile acid transport and canalicular membrane integrity in mice. Biochemical Journal. 2011; 434:49–60. [PubMed: 21118154]
25. Masedunskas A, Sramkova M, Parente L, Sales KU, Amornphimoltham P, Bugge TH, Weigert R. Role for the actomyosin complex in regulated exocytosis revealed by intravital microscopy. Proc Natl Acad Sci U S A. 2011; 108:13552–13557. [PubMed: 21808006]
26. Aijaz S, D'Atri F, Citi S, Balda MS, Matter K. Binding of GEF-H1 to the tight junction-associated adaptor cingulin results in inhibition of Rho signaling and G1/S phase transition. Dev Cell. 2005; 8:777–786. [PubMed: 15866167]
27. Ducommun S, Deak M, Sumpton D, Ford RJ, Nunez Galindo A, Kussmann M, Viollet B, et al. Motif affinity and mass spectrometry proteomic approach for the discovery of cellular AMPK targets: identification of mitochondrial fission factor as a new AMPK substrate. Cell Signal. 2015; 27:978–988. [PubMed: 25683918]
28. Gissen P, Arias IM. Structural and Functional Hepatocyte Polarity and Liver Disease. J Hepatol. 2015
29. Ryan JC, Ghabril M, Decker B, Dunn K. Quantitative Intravital Microscopy of Liver Transport. Molecular Biology of the Cell. 2012:23.
30. Weigert R, Porat-Shliom N, Amornphimoltham P. Imaging cell biology in live animals: ready for prime time. J Cell Biol. 2013; 201:969–979. [PubMed: 23798727]
31. Larina O, Bhat P, Pickett JA, Launikonis BS, Shah A, Kruger WA, Edwardson JM, et al. Dynamic regulation of the large exocytotic fusion pore in pancreatic acinar cells. Molecular Biology of the Cell. 2007; 18:3502–3511. [PubMed: 17596517]

32. Xiang RL, Mei M, Cong X, Li J, Zhang Y, Ding C, Wu LL, et al. Claudin-4 is required for AMPK-modulated paracellular permeability in submandibular gland cells. Journal of Molecular Cell Biology. 2014; 6:486–497. [PubMed: 25503106]
33. Toyama EQ, Herzig S, Courchet J, Lewis TL Jr, Loson OC, Hellberg K, Young NP, et al. Metabolism. AMP-activated protein kinase mediates mitochondrial fission in response to energy stress. Science. 2016; 351:275–281. [PubMed: 26816379]
34. Lizcano JM, Goransson O, Toth R, Deak M, Morrice NA, Boudeau J, Hawley SA, et al. LKB1 is a master kinase that activates 13 kinases of the AMPK subfamily, including MARK/PAR-1. Embo Journal. 2004; 23:833–843. [PubMed: 14976552]
35. Nakano A, Kato H, Watanabe T, Min KD, Yamazaki S, Asano Y, Seguchi O, et al. AMPK controls the speed of microtubule polymerization and directional cell migration through CLIP-170 phosphorylation. Nature Cell Biology. 2010; 12:583–U139. [PubMed: 20495555]
36. Hardie DG. AMP-activated protein kinase-an energy sensor that regulates all aspects of cell function. Genes & Development. 2011; 25:1895–1908. [PubMed: 21937710]
37. Nunnari J, Suomalainen A. Mitochondria: In Sickness and in Health. Cell. 2012; 148:1145–1159. [PubMed: 22424226]
38. Mihaylova MM, Shaw RJ. The AMPK signalling pathway coordinates cell growth, autophagy and metabolism. Nature Cell Biology. 2011; 13:1016–1023. [PubMed: 21892142]
39. Fu D, Mitra K, Sengupta P, Jarnik M, Lippincott-Schwartz J, Arias IM. Coordinated elevation of mitochondrial oxidative phosphorylation and autophagy help drive hepatocyte polarization. Proc Natl Acad Sci U S A. 2013; 110:7288–7293. [PubMed: 23589864]
40. Derangeon M, Spray DC, Bourmeyster N, Sarrouilhe D, Herve JC. Reciprocal influence of connexins and apical junction proteins on their expressions and functions. Biochimica Et Biophysica Acta-Biomembranes. 2009; 1788:768–778.
41. Fanning AS, Anderson JM. Zonula Occludens-1 and-2 Are Cytosolic Scaffolds That Regulate the Assembly of Cellular Junctions. Molecular Structure and Function of the Tight Junction: From Basic Mechanisms to Clinical Manifestations. 2009; 1165:113–120.
42. Guillot C, Lecuit T. Mechanics of epithelial tissue homeostasis and morphogenesis. Science. 2013; 340:1185–1189. [PubMed: 23744939]
43. Buschmann MM, Shen L, Rajapakse H, Raleigh DR, Wang Y, Wang Y, Lingaraju A, et al. Occludin OCEL-domain interactions are required for maintenance and regulation of the tight junction barrier to macromolecular flux. Molecular Biology of the Cell. 2013; 24:3056–3068. [PubMed: 23924897]
44. Clayburgh DR, Barrett TA, Tang Y, Meddings JB, Van Eldik LJ, Watterson DM, Clarke LL, et al. Epithelial myosin light chain kinase-dependent barrier dysfunction mediates T cell activation-induced diarrhea in vivo. J Clin Invest. 2005; 115:2702–2715. [PubMed: 16184195]
45. Anderson JM. Leaky junctions and cholestasis: a tight correlation. Gastroenterology. 1996; 110:1662–1665. [PubMed: 8613080]
46. Schossleitner K, Rauscher S, Groger M, Friedl HP, Finsterwalder R, Habertheuer A, Sibilia M, et al. Evidence That Cingulin Regulates Endothelial Barrier Function In Vitro and In Vivo. Arterioscler Thromb Vasc Biol. 2016
47. Hanzon V. Liver cell secretion under normal and pathologic conditions studied by fluorescence microscopy on living rats. Acta Physiol Scand Suppl. 1952; 28:1–268. [PubMed: 13007504]
48. Porat-Shliom N, Chen Y, Tora M, Shitara A, Masedunskas A, Weigert R. In vivo tissue-wide synchronization of mitochondrial metabolic oscillations. Cell Rep. 2014; 9:514–521. [PubMed: 25373899]

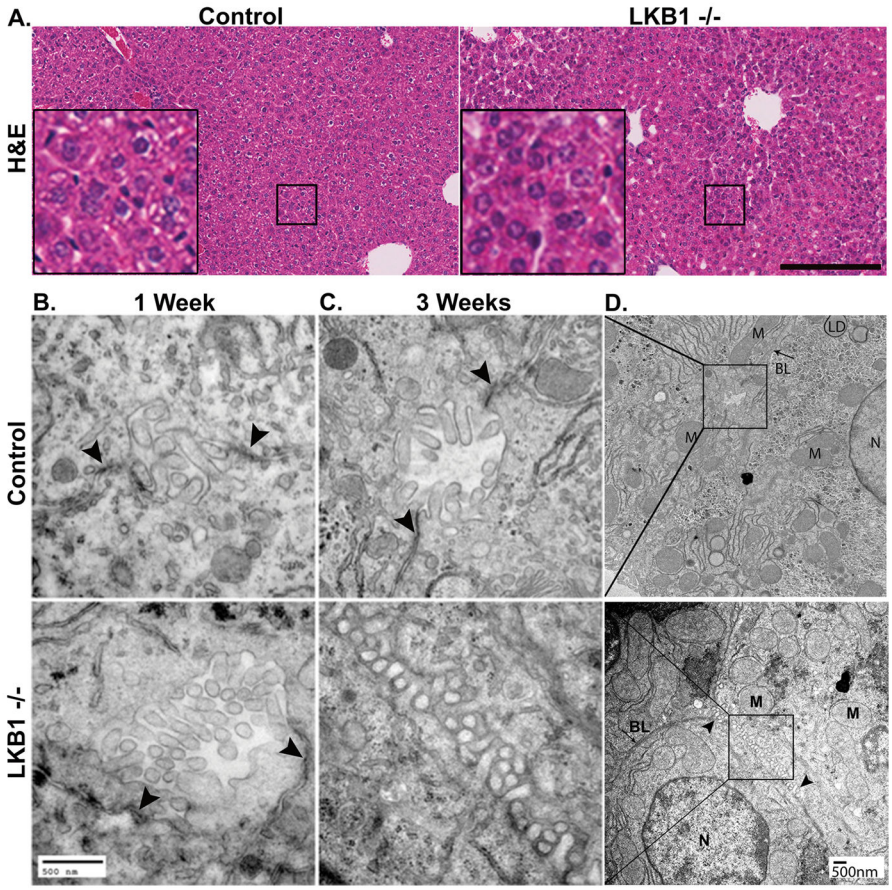

Figure 1. Hepatocytes and tissue architecture in control and LKB1 −/− mice

A. Livers from 3-week old control and LKB1 −/− mice were stained with H&E. Scale bar: 200μm. **B.** TEM of liver sections from 1-week control and LKB1 −/− mice (upper and lower panel, respectively). Arrowheads indicate TJs. **C.** TEM of liver sections from 3-week control and LKB1 −/− mice (upper and lower panel, respectively). Arrowheads indicate TJs in control (upper panel). In LKB1 −/− (lower panel) bile canaliculi morphology was altered. **D.** Lower magnification of the insets shown in C. N=Nucleus; M=Mitochondria; BL=Basolateral; LD=Lipid droplet. Scale bar: 500nm.

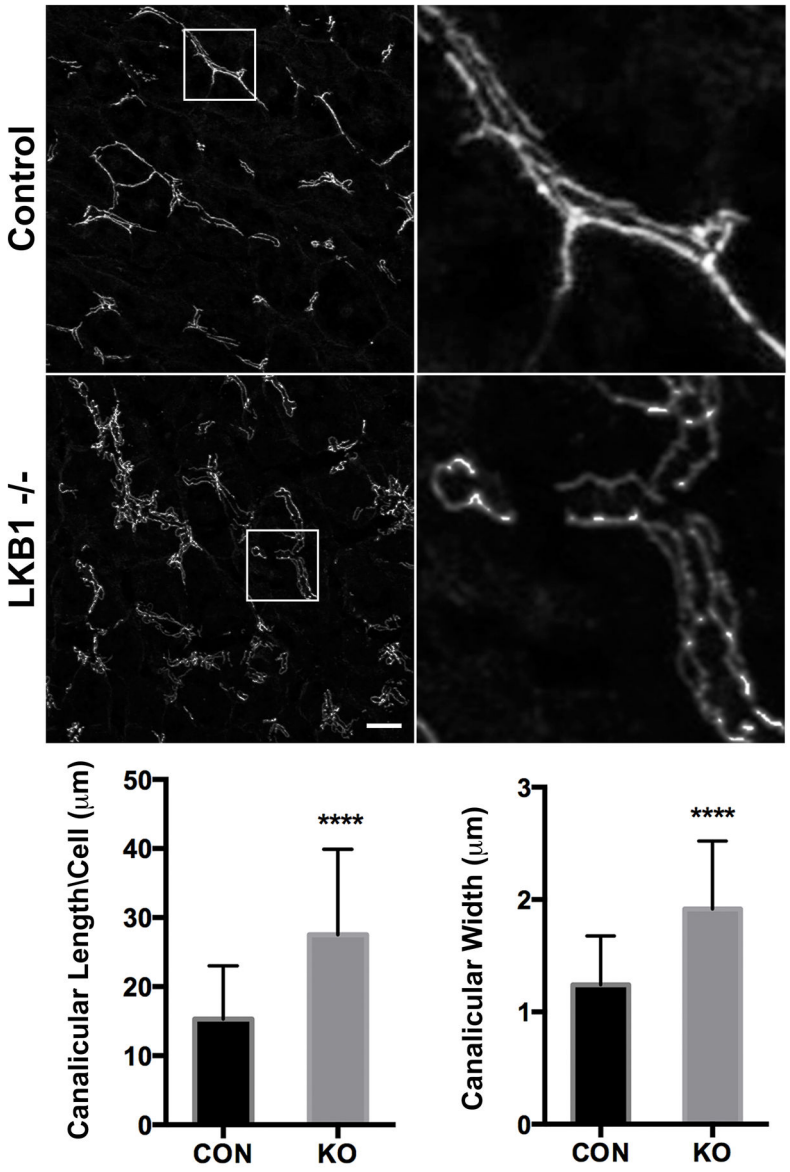

Figure 2. Loss of LKB1 leads to changes in canalicular morphology

Liver sections were stained with ZO-1 antibody. Scale bar: 10μm. ZO-1 labeling was used for indirect evaluation of canalicular width and length. For canalicular width, mean of 1.24 ± 0.08 (N=29) was measured in control (black bar) while 1.91 ± 0.1 (N=36) was measured in LKB1 −/− (grey bar) sections $p < 0.0001$. For canalicular length, mean of 15.30 ± 1.17 (N=43) was measured in control (black bar) while 27.53 ± 2.12 (N=34) was measured in LKB1 −/− (grey bar) sections $p < 0.0001$. Similar results were obtained from three independent experiments.

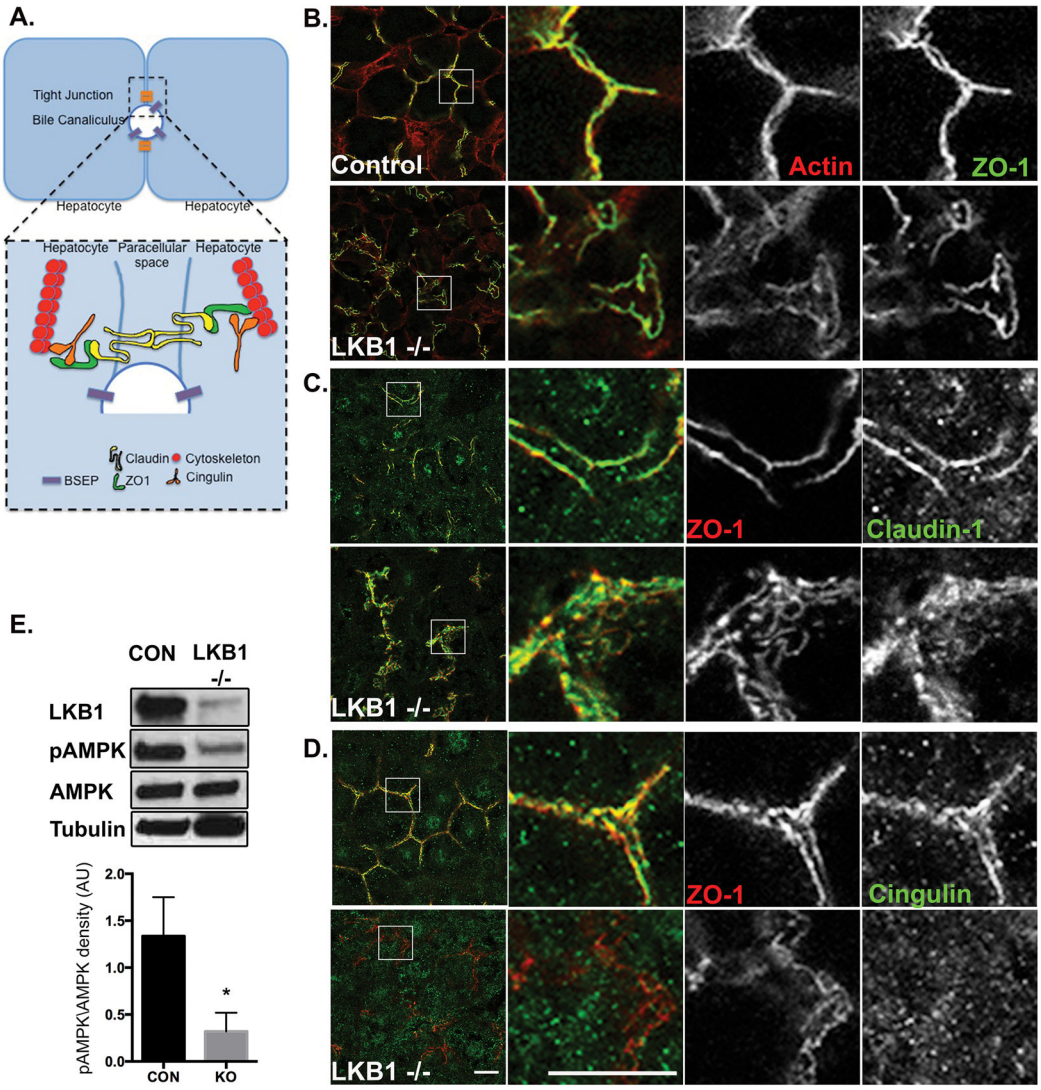

Figure 3. Loss of LKB1 leads to disruption of TJ components and reduced AMPK activation

A. Simplified schematic representation of TJ organization in hepatocytes. TJs are at the interface of lateral and apical membranes and are composed of transmembrane proteins (claudin; yellow), scaffold proteins (ZO-1; green), regulatory proteins (cingulin; orange) and cytoskeleton (actin or microtubules; red). **B-D.** Liver sections from control (upper panels) or LKB1 −/− (lower panels) were stained with phalloidin, Claudin-1 or Cingulin and ZO-1 antibodies. Note the redistribution of cingulin to the cytosol in LKB1 −/− as compared with control. Scale bar: 10μm. **E.** Western blot analysis of LKB1, AMPK and pAMPK. Total cell lysates of livers from control and LKB1 −/− mice were immunoblotted to determine levels of LKB1, AMPK, and phospho-Thr172 AMPK (pAMPK). Representative Western blots are shown. Quantification of pAMPK/AMPK from three independent experiments was plotted as Mean ± SEM (control 1.33 ± 0.23; LKB1 −/− 0.31 ±0.11; $p < 0.005$).

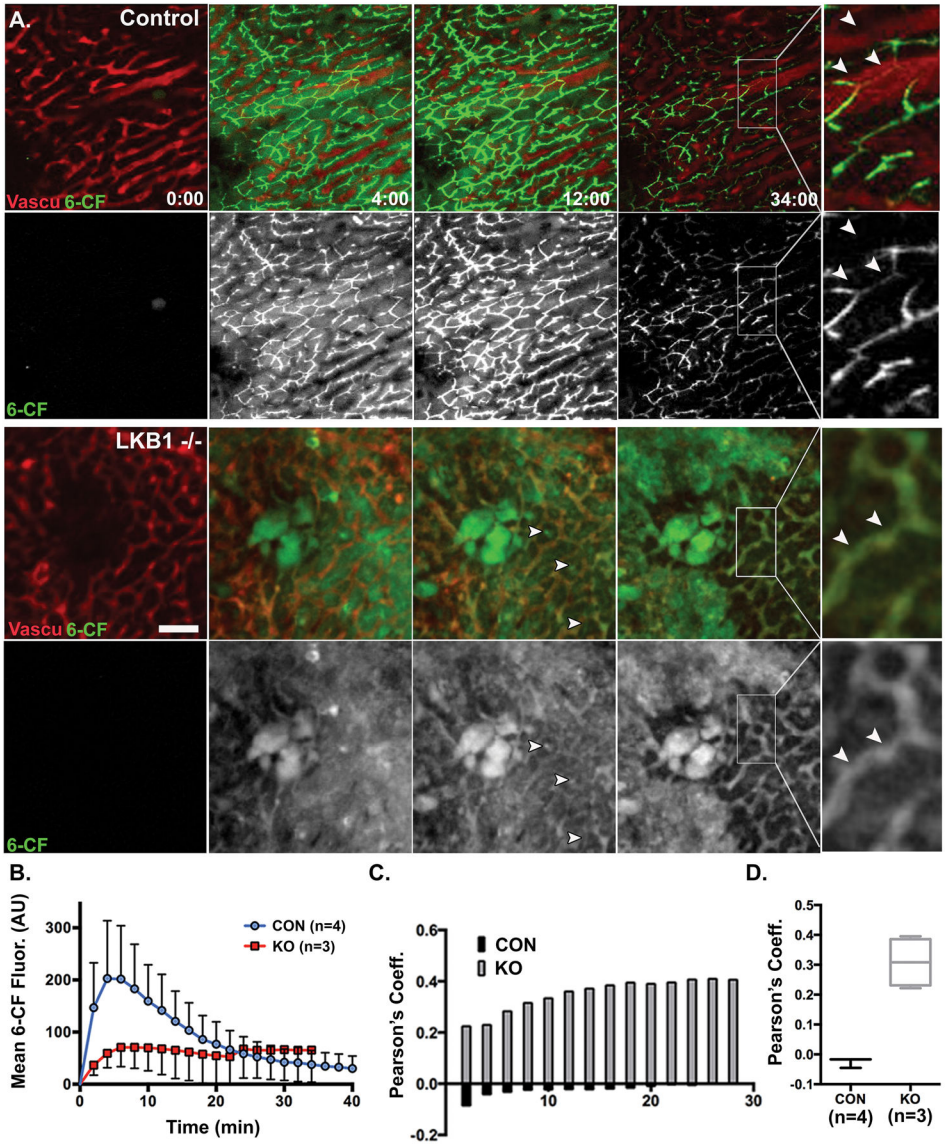

Figure 4. IVM of biliary excretion in the intact liver

A. Mice were anesthetized and positioned on the microscope stage for IVM of the liver as described in Materials and Methods. Single frames from time-lapse imaging of control (upper panel) or LKB1 −/− (lower panel) are presented. Blood flow and sinusoid space were visualized with Qtracker 655 probe (red) that was injected systemically prior to imaging. To measure biliary excretion, 6-CFDA (green) was injected following the acquisition of the first z-stack. Note that canaliclar structures were fewer in LKB1 −/− (arrowheads) and 6-CF signal from hepatocytes was observed throughout suggesting delayed excretion compared with control. Inset: Qtracker and 6-CF label the vasculature and canaliculi, respectively in control, in LKB1 −/− they overlapped in blood vessels (white arrowheads). Scale bar: 50μm. **B.** Measurement of 6-CF Mean + SEM fluorescence in control (blue; n=4 mice) and LKB1 −/− (red; n=3 mice) are plotted. **C.** The degree of co-localization of Qtracker (red) and 6-CF (green) was quantified and expressed as Pearson co-localization coefficient (1, perfect

correlation; 0, no correlation; and −1, inverse correlation). Representative Pearson's coefficient values from control (black bars) or LKB1 −/− (grey bars) over time. **D.** Pearson's coefficient values at t=34 minutes from control (black; n=4 mice) or LKB1 −/− (grey; n=3 mice).

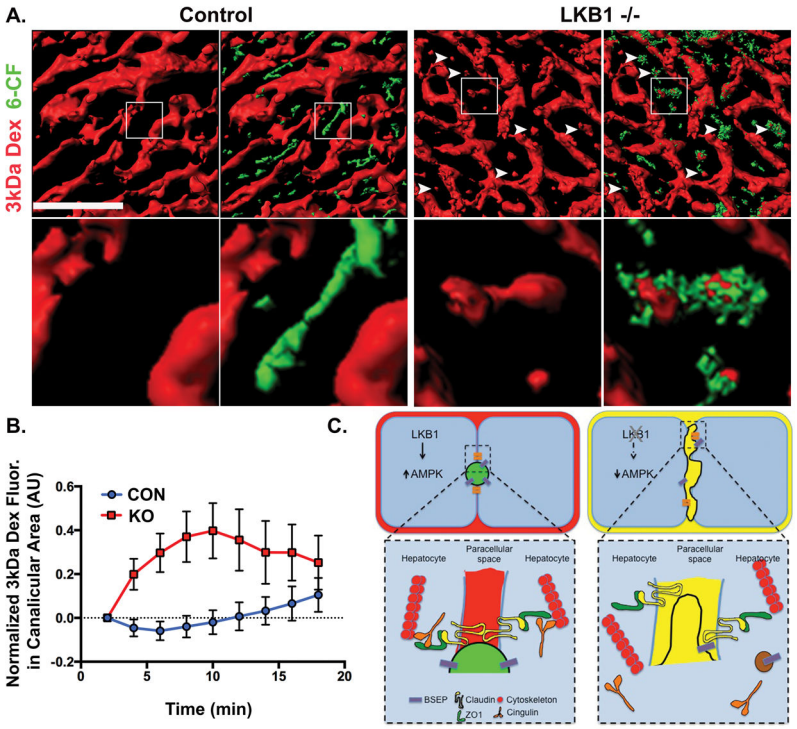

Figure 5. IVM of TJs permeability and the paracellular pathway

A. Mice were anesthetized and positioned on the microscope stage for IVM of the liver as described in Materials and Methods. Blood flow and sinusoid space were visualized with Qtracker 655 probe (not shown) that was injected systemically prior to imaging. 3kDa dextran (red) and 6-CFDA (green) were injected following the acquisition of the first z-stack. Volume rendering of the different probes were generated and a single frame of 3kDa dextran or an overlay of 3kDa and 6-CF are shown. Enlarged inset in lower panel corresponds to the boxed area in the panel above. Note that in LKB1 −/−, but not control, 3kDa dextran is present in the canaliculi area also labeled by 6-CF (white arrowheads). Scale bar: 50μm. **B.** Measurement of 3kDa dextran Mean ± SD of 20 regions in the bile canaliculi area was plotted for representative control (blue) or LKB1 −/− (red). Similar results were obtained in three independent experiments. **C.** Proposed model summarizing experimental observations. LKB1 deficient mice have reduced levels of phosphorylated AMPK levels, which may be the cause of the observed abnormal canaliculi morphology and distribution of TJ proteins. Notably, the apical pole extends into the lateral domain of hepatocytes and the junctional regulatory protein, cingulin (orange) localizes primarily in the cytosol. Mis-localization of additional TJ proteins, membrane trafficking regulators and BSEP may explain the delayed biliary excretion. Finally, mixing of biliary (green in control) and blood (red in control) content (represented as yellow) is observed in mice lacking LKB1.